Manipulation of liquid droplets in a planar platform using periodic thermocapillary actuation

Z. J. Jiao, X. Y. Huang and N. -T. Nguyen
School of Mechanical and Aerospace Engineering
Nanyang Technological University
Singapore

Receipt/Acceptance Data **[DO NOT ALTER/DELETE THIS TEXT]**
Publication data **[DO NOT ALTER/DELETE THIS TEXT]**
DOI: 10.1039/b000000x [DO NOT ALTER/DELETE THIS TEXT]

A manuspcript submitted to Lab on a Chip

10 pages, 9 figures.

Abstract

Thermocapillary manipulation of droplets in a planar platform with periodic actuation has been demonstrated by both theoretical simulation and experimental characterization. The driving temperature gradients are provided by four micro heaters embedded at boundaries of the planar platform. The temperature distributions corresponding to the periodic actuations are calculated, then coupled with the temperature-dependent surface tensions to derive the droplet motion. The results show that the droplet is driven along various closed-loops whose patterns can be designed and controlled by the periodic heating schemes and actuation frequencies. Qualitative agreement between the simulation and experimental observation, in terms of the temperature distributions and droplet moving trajectories, has been obtained. The concept of the droplet manipulation presented in this paper has potential applications in droplet-based lab-on-a-chip systems.

Keywords: lab on a chip; droplet; thermocapillarity; droplet-based microfluidics; digital microfluidics.

Introduction

Life science research using micro-scale tools has a growing importance in the last decade, where droplet-based microfluidics began emerging as an alternative for bio-chemical analysis processes. A good option for the carrier of reagents in microchannels is the microdroplet, which also provides a platform for chemical reactions. The emerging field of droplet-based microfluidics leads to a need for effective and flexible manipulations of individual droplets in microscale[1]. Most of the reported droplet-based microfluidic devices used continuous-flow platforms based on microchannels. Active control of microdroplets were achieved by pressure differences [2], thermocapillarity [3], electrowetting [4] or other effects. Comparing with continous-flow platforms, a two dimensional (2D) planar platform handles droplets individually with greater flexibilities [4]. The actuation may be achieved through chemical or thermal gradients [5], surface acoustic waves [6], and electric fields [4, 7]. Manipulation of droplets by thermal gradient actuation was reported previously by Darhuber et. al [8, 9]. In their work, a complex programmable multi-heaters array design was used to achieve motion control of the droplet. The micro-heaters allowed the control of the surface temperature distribution with high spatial

resolutions. Combined with chemical surface patterning, the device can be used as a logistic platform for the parallel and automated routing, mixing and reacting of a number of liquid samples.

Thermocapillary control of microdroplets were also obtained by our group using boundary-heaters with programmable heating schemes[10-13]. In these studies, simulations and experiments were conducted on the one-dimensional (1D) dynamics of a liquid plug actuated between two heaters in a straight capillary. The actuation concept allowed both transient and reciprocating motions of the liquid plug. In the study presented in this paper, the 1D model for the periodic thermocapillary actuation in capillary tubes is extended to a 2D planar square platform with four heaters at the edges. The liquid droplet is positioned between two glass plates. The bottom plate contains the four driving heaters, while the top plate defines the height of the platform. Compared to the works reported by Fair [4] and Darhuber et. al [8, 9], our concept is easier in its fabrication and implementation. In our concept, the square area bounded by the heaters is considered to be much larger than the droplet size. Temperature distributions in the square region are realized spatially with four controllable heating boundary conditions. Through the coupling of the temperature field and the surface tension, the droplet's motion and position can be controlled. The results presented in this paper demonstrate that complete manipulation of the droplet in an arbitrary region can be achieved by various heating schemes and different actuation frequencies at its boundary.

Theoretical modelling

Temperature distributions

Figure 1 shows the schematic concept of the thermocapillary actuation of an individual droplet in a planar platform. In order to simplify the model, a square region of $a \times a$ has been considered in this study. The temperature distribution inside the platform can be described by the following governing equation,

$$\frac{\partial \theta}{\partial t} = \alpha \left(\frac{\partial^2 \theta}{\partial x^2} + \frac{\partial^2 \theta}{\partial y^2} \right) - \frac{h}{H \rho c} \theta , \tag{1}$$

where θ is the temperature difference relative to the ambient temperature, H is the thickness of the substrate plane, α, ρ, h and c are the thermal diffusivity, density, convection coefficient and specific heat capacity of the substrate material respectively. Heat radiation is negligible in this model because

of the relatively low temperature of the substrate surface. The boundary conditions are

$$\begin{cases} \dfrac{\partial\theta}{\partial x}|_{x=0} = -f_1(t)\dfrac{q_0^{"}}{k} \\ \dfrac{\partial\theta}{\partial x}|_{x=a} = f_2(t)\dfrac{q_0^{"}}{k} \end{cases}, \quad \begin{cases} \dfrac{\partial\theta}{\partial y}|_{y=0} = -f_3(t)\dfrac{q_0^{"}}{k} \\ \dfrac{\partial\theta}{\partial y}|_{y=a} = f_4(t)\dfrac{q_0^{"}}{k} \end{cases} \tag{2}$$

where q_0'' is the maximum heat flux that can be supplied by an individual heater and k is the conductivity of the substrate material. $f_1(t)$, $f_2(t)$, $f_3(t)$ and $f_4(t)$ are time-dependent factors controlling four heaters respectively. In the periodic actuation, we assume that all heaters are activated periodically with the same period, T_h. By introducing the dimensionless variables $\theta^* = \theta k / q_0^{"} a$, $x^* = x/a$, $t^* = t/T_h$, we have the dimensionless heat transfer equation and boundary conditions

$$\eta\frac{\partial\theta^*}{\partial t^*} = \alpha\left(\frac{\partial^2\theta^*}{\partial x^{*2}} + \frac{\partial^2\theta^*}{\partial y^{*2}}\right) - \xi\theta^*, \tag{3}$$

$$\begin{cases} \dfrac{\partial\theta^*}{\partial x^*}|_{x^*=0} = f_1(t^*) \\ \dfrac{\partial\theta^*}{\partial x^*}|_{x^*=1} = f_2(t^*) \end{cases}, \quad \begin{cases} \dfrac{\partial\theta^*}{\partial y^*}|_{y^*=0} = f_3(t^*) \\ \dfrac{\partial\theta^*}{\partial y^*}|_{y^*=1} = f_4(t^*) \end{cases}, \tag{4}$$

where $\eta = a^2/(\alpha T_h)$ and $\xi = ha^2/Hk$. In order to homogenize the time-dependent boundary conditions, we set

$$f(x^*, y^*, t^*) = x^* f_1(t^*) + \frac{x^{*2}}{2}\left[f_2(t^*) - f_1(t^*)\right] + y^* f_3(t^*) + \frac{y^{*2}}{2}\left[f_4(t^*) - f_3(t^*)\right], \tag{5}$$

such that

$$\begin{cases} \dfrac{\partial f}{\partial x^*}|_{x^*=0} = f_1(t^*) \\ \dfrac{\partial f}{\partial x^*}|_{x^*=1} = f_2(t^*) \end{cases}, \quad \begin{cases} \dfrac{\partial f}{\partial y^*}|_{y^*=0} = f_3(t^*) \\ \dfrac{\partial f}{\partial y^*}|_{y^*=1} = f_4(t^*) \end{cases}. \tag{6}$$

By setting

$$\theta^*(x^*, y^*, t^*) = g(x^*, y^*, t^*) + f(x^*, y^*, t^*) \tag{7}$$

and substituting eqs.(5) and (7) into eq. (3), we have

$$\frac{\partial g}{\partial t^*}=\alpha\left(\frac{\partial^2 g}{\partial x^{*2}}+\frac{\partial^2 g}{\partial y^{*2}}\right)-\xi g+\left[\, f_2(t^*)-f_1(t^*)+f_4(t^*)-f_3(t^*)\right]-\xi f\,, \tag{8}$$

$$\begin{cases}\dfrac{\partial g}{\partial x^*}|_{x^*=0}=0\\ \dfrac{\partial g}{\partial x^*}|_{x^*=1}=0\end{cases},\quad \begin{cases}\dfrac{\partial g}{\partial y^*}|_{y^*=0}=0\\ \dfrac{\partial g}{\partial y^*}|_{y^*=1}=0\end{cases}. \tag{9}$$

Function $g(x^*,y^*,t^*)$ can be expanded by the Fourier series according to the homogeneous boundary conditions (9) and the periodic characteristics, and are solved from eq. (8). The final temperature distribution is obtained as

$$\begin{aligned}&\theta^*(x^*,y^*,t^*)=g(x^*,y^*,t^*)+f(x^*,y^*,t^*)\\&=\sum_{N=-\infty}^{\infty}g_{00N}e^{i2\pi Nt^*}+\sum_{m=1}^{\infty}\sum_{N=-\infty}^{\infty}g_{m0N}\cos(m\pi x^*)e^{i2\pi Nt^*}+\sum_{n=1}^{\infty}\sum_{N=-\infty}^{\infty}g_{0nN}\cos(n\pi y^*)e^{i2\pi Nt^*}\\&+x^*f_1(t^*)+\frac{x^{*2}}{2}\left[\, f_2(t^*)-f_1(t^*)\right]+y^*f_3(t^*)+\frac{y^{*2}}{2}\left[\, f_4(t^*)-f_3(t^*)\right],\end{aligned} \tag{10}$$

where

$$\begin{cases}g_{00N}=\dfrac{d_{00N}-(i2\eta\pi N+\xi)f_{00N}}{i2\eta\pi N+\xi}\\ g_{m0N}=\dfrac{-(i2\eta\pi N+\xi)f_{m0N}}{i2\eta\pi N+\xi+m^2\pi^2}\\ g_{0nN}=\dfrac{-(i2\eta\pi N+\xi)f_{0nN}}{i2\eta\pi N+\xi+n^2\pi^2}\end{cases} \tag{11}$$

and

$$\begin{cases}d_{00N}=\displaystyle\int_0^1\left[\, f_2(t^*)-f_1(t^*)+f_4(t^*)-f_3(t^*)\right]e^{-i2\pi Nt^*}dt^*\\ f_{00N}=\displaystyle\int_0^1\int_0^1\int_0^1 fe^{-i2\pi Nt^*}dx^*dy^*dt^*\\ f_{m0N}=2\displaystyle\int_0^1\int_0^1\int_0^1 f\cos(m\pi x^*)e^{-i2\pi Nt^*}dx^*dy^*dt^*\\ f_{0nN}=2\displaystyle\int_0^1\int_0^1\int_0^1 f\cos(n\pi y^*)e^{-i2\pi Nt^*}dx^*dy^*dt^*\end{cases} \tag{12}$$

Coupling of temperature field with droplet motion

The temperature distributions in the platform are coupled to the droplet motion through surface tensions. The unbalanced surface tensions on the droplet, due to the temperature gradients, drive the droplet moving inside the platform. The surface tension σ_{lg} of the liquid depends on the temperature. For a small temperature range, a linear relation can be assumed as

$$\sigma_{\mathrm{lg}}(\theta) = \sigma_{\mathrm{lg}0} - \varepsilon(\theta - \theta_0), \tag{13}$$

where $\sigma_{\mathrm{lg}0}$ is the liquid-gas surface tension at the reference temperature θ_0 and ε is the temperature coefficient of surface tension. The temperature field resulting from eq. (1) is a function of time and position (x, y, t). Assuming a weak thermal interaction between the droplet and the substrate surface, the surface tension can be described as a function of time and position through the temperature distributions

$$\sigma_{\mathrm{lg}}(\theta) = f[\theta(x,y,t)] = \sigma_{\mathrm{lg}}(x,y,t). \tag{14}$$

Since the droplet diameter $2R$ is normally smaller than the Laplace length $\kappa^{-1}(\kappa^2 = \rho g/\sigma_{\mathrm{lg}})$, the droplet shape is assumed to be circular, the radius of curvature constant and the dynamic contact angle uniform along the contact line. The dominant viscous dissipation occurs in the bulk for flat structures, and the dissipation at the solid-liquid-gas contact line is negligible. With the lubrication approximation, the viscous drag force generated within the liquid is [14]

$$\begin{cases} F_{vx} = 3\mu u \int_M^N \dfrac{dx}{\lambda(x)} = \dfrac{6\mu u R}{h_g} \\ F_{vy} = 3\mu v \int_M^N \dfrac{dy}{\lambda(y)} = \dfrac{6\mu v R}{h_g} \end{cases}, \tag{15}$$

where $\lambda(x)$ is the droplet height profile function, u, v are the velocity magnitudes in x and y directions respectively, μ is the liquid viscosity, R is the the droplet base radius, and h_{g} is the gap between the two glass plates. The liquid viscosity, based on the previous work of Yarin, is dependent on temperature at the droplet center[15],

$$\mu = \mu_0 \exp\left[3.8 T_b \left(\frac{1}{T_{\mathrm{center}}} - \frac{1}{T_0}\right)\right], \tag{16}$$

where μ_0 is the viscosity at some reference temperature T_0 (normally 293K), T_b is the liquid boiling temperature, and T_{center} is the absolute temperature at the droplet center (θ + ambient temperature in

the present study). In order to make the droplet evaporate imperceptible and reduce hysteretic effects, silicone oil was chosen to be the droplet liquid. In this case, we have the capillary number $Ca = \frac{\mu U}{\sigma_{\lg}} < 1\times10^{-3}$ where the velocity is less than 1 mm/s. The low capillary number ensures that the moving droplet has a nearly constant circular profile, and the dynamic contact angles are assumed to be constant for purpose of simplification. The circular perimeter of the droplet is divided into *n* finite elements, the resultant force on both *x*, and *y* directions can be calculated by combining all the surface tension forces acting on the individual sector,

$$\begin{cases} F_x = 2\sum_{i=1}^{n} \frac{2\pi R}{n} \cos\left[\frac{(2i+1)n}{n}\right] \sigma_{\lg}(x_i, y_i, t) \\ F_y = 2\sum_{i=1}^{n} \frac{2\pi R}{n} \sin\left[\frac{(2i+1)n}{n}\right] \sigma_{\lg}(x_i, y_i, t) \end{cases} \tag{17}$$

where $\sigma_{\lg}(x_i, y_i, t) = \sigma_{\lg}\left(x_0 + R\cos\frac{\pi(2i+1)}{n}, y_0 + R\sin\frac{\pi(2i+1)}{n}, t\right)$, (x_0, y_0) is the initial droplet position. A larger *n* leads to a more accurate result. In the present study, the number of the finite elements was set at *n* = 8. The velocity $U = u\hat{x} + u\hat{y}$ can be determined by the force balance between the inertia, friction and thermocapillary force, i.e.,

$$\begin{cases} \rho V \frac{\mathrm{d}u}{\mathrm{d}t} = -\frac{6\mu R}{h_g} u + F_x \\ \rho V \frac{\mathrm{d}v}{\mathrm{d}t} = -\frac{6\mu R}{h_g} v + F_y \end{cases} \tag{18}$$

Here *u* and *v* are the velocity components in the x-axis and y-axis directions respectively. V is the volume of the droplet ($V \approx \pi R^2 h_g$). The dynamic contact angle along the contact line is assumed to be the same as the static contact angle, which is about 10^o. By setting $A = \frac{6\mu R}{\rho V h_g}$, $B_x = -\frac{F_x}{\rho V}$ and $B_y = -\frac{F_y}{\rho V}$, the velocity of the droplet can be solved as

$$\begin{cases} u = -\frac{B_x}{A} + \frac{B_x}{A} e^{-At} \\ v = -\frac{B_y}{A} + \frac{B_y}{A} e^{-At} \end{cases}. \tag{19}$$

Experiments setup and materials

The experimental setup is illustrated in Figure 2. The planar platform was formed between two glass plates. The gap between the plates was 0.5 mm. Four titanium/platinum microheaters were sputtered and structured on the bottom glass plate along the four sides of a 10 mm × 10 mm square region. The droplet was actuated within this square region. In the experiments, the maximum heating power was kept at 0.5 W for all heaters. An in-house built circuit was used to control the individual heater according to the required heating scheme. These heating signals were also used to trigger a CCD camera for capturing the droplet motion images. The CCD camera was operated at rate of two frames per second throughout the experiments. The resolution of the camera was 640 pixels × 480 pixels. A thermal tracer camera (NEC TH9100PMVI) was used for the temperature distribution measurement. Silicone oils PDMS (polydimethylsiloxane, Sigma Aldrich) of viscosity 10 cSt was used in the experiments as the working liquid for the droplets, and the droplet radius was kept at 0.5-0.7 mm. The density, surface tension at room temperature (20 °C), temperature coefficient of the surface tension are ρ = 930 kg/m3, σ_{lg0} = 20.3 mN/m and ε = 0.06 mN/mK , respectively. The droplet was injected into the planar platform by a precision syringe.

Results and discussions

In the following, the simulation results are presented and discussed. A part of them are subsequently verified and compared with the experimental characterizations.

Simulation results

In the periodic actuation, we consider the situation that the heaters have been switched on for a long time and the periodic temperature distributions have been established inside the square glass plate. The temperature variations depend on the heating scheme within one period. Figure 3 shows a typical case, in which one period is divided into four quarters and each heater works only in one quarter period, as shown in Figure 3(a). The corresponding temperature distributions in each quarter period are plotted in Figures 3(b)-(e). In this case, a droplet introduced into the platform will be driven to move in a loop as illustrated in Figure 4(a). The periodic motion of the droplet is better observed by plotting its displacement and temperature in Figures 4(b) and (c) respectively. It is interesting to note that the

droplet experiences a quick change from low temperature to high temperature in each period, which is depicted in Figure 4(d). Three different periodic heating schemes and the corresponding droplet moving patterns are illustrated in Figure 5. A variety of loop patterns for the droplet moving inside the platform can be generated by different periodic heating schemes.

Experimental characterization

The experimental characterizations of the droplet under periodic thermocapillary actuation were conducted to verifiy the simulation results, and also to demonstrate the the possibility of achieving periodic droplet manipulation. Figure 6 shows the measured periodic temperature distributions in four quarters of a single period, captured by the thermal tracer camera. Except for the low temperatures at the four corners, experimental results (Figure 6) agree relatively well with the theoretical results (Figure 3). The discrepancy is caused by the lack of heat generation at the corners. Under this heating scheme, Figure 7 shows the captured images of the silicon oil droplet at different time instances, the corresponding trajectory and the displacements versus time. In comparison to the results depicted in Figures 4(a) and 4(b), we can see a qualitative agreement between the simulation and experimental results in terms of trajectories and time-dependent position of the droplet. Three other heating schemes, as shown and theoretically predicted in Figure 5, were tested in the experiment with the same period T_h = 80s. The results are presented in Figure 8, illustrated by selected images in one period and trajectories obtained from the recorded images. It is seen that the trajectories are similar to those closed-loop trajectories theoretically predicted in Figure 5. The effect of the heating period on droplet motions was studied in the experiment by actuating a droplet with the same heating scheme but in different periods. The results are shown in Figure 9. The main differences are in the loop sizes and the corner shapes. The longer period leads to a larger loop with sharp corners, while a shorter period results in a smaller loop with rounded perimeters, indicating that the actuation period or the frequency is a parameter to control the trajectory shapes.

Conclusions

The periodic thermocapillary actuation of droplet inside a planar platform has been simulated and experimentally verified. The heaters are located at the platform edges. The results show that, under the periodic actuation, the droplet can be driven to move in a closed loop whose pattern is controlled by the periodic heating schemes and actuation frequencies. Under various heating schemes, the droplet can be manipulated with great flexibility. In terms of temperature distributions and droplet trajectories,

qualitative agreement between the simulation and the experimental results has been achieved. The actuation concepts reported in this paper may offer an alternative platform for the droplet processes and would have potential applications in droplet-based microfluidics, such as thermal cycling of deoxyribonucleic acid (DNA) molecules contained within a liquid droplet.

Acknowledgement

The authors would like to thank the Academic Research Fund of the Ministry of Education Singapore (grant no RG26/06) for its financial support.

References

1. H. Song, D.L. Chen, R.F. Ismagilov, Angew. *Chem. Int. Ed*., 2006, **45,** 7336-7356.
2. D. Link, S. L. Anna, D. Weitz, H. A. Stone, *Physical Review Letters*, 2004, **92**, 054503.
3. T. H. Ting, Y. F. Yap, N. T. Nguyen, T. N. Wong, J.C.K. Chai, L. Yobas, *Applied Physics Letter*, 2006, **89**, 234101.
4. R. B. Fair, *Microfluid. Nanofluid.*, 2007, **3**, 245-281.
5. F. Brochard, *Langmuir*, 1988, **5**, 432.
6. C. J. Stroll, A. Rathgeber, A. Wixforth, C. Gauer, J. Scriba, 2002, *IEEE Ultrasonics Symposium*, **2002**, 258.
7. O. D. Velev, B. G. Prevo, K. H. Bhatt, *Nature*, 2003, **424**, 515-516.
8. AA. Darhuber, J. M. Davis, S. M. Troian, W. W. Reisner, *Phys. Fluids*, 2003, **15**, 1295-304.
9. A. Darhuber, J. P. Valentino, S. M. Troian, S. Wagner, *J. Microelectromech. Syst*, 2003, **12**, 873-79.
10. N. T. Nguyen and X. Y. Huang, *Japanese Journal of Applied Physics*, 2005, **94**, 1139-1142.
11. Z. Jiao, N. T. Nguyen, X. Y. Huang, A. Z. Ang, *Microfluidics and Nanofluidics*, 2007, **3(1)**, 39-46.
12. Z. Jiao, N. T. Nguyen, X. Y. Huang, *Journal of Micromechanics and Microengineering*, 2007, **17(9),** 1843-1852.
13. Z. Jiao, N. T. Nguyen, X. Y Huang, *Sensors and Actuators A*, 2007, DOI: 10.1016/j.sna.2007.06.025.
14. S. Daniel, M. K. Chaudhury, *Langmuir*, 2002, **18**, 3404-3407.

15. A. L. Yarin, W. X. Liu and D. H. Reneker, *Intel society conference on thermal phenomena*, 2002, **91**,7.

List of Figures

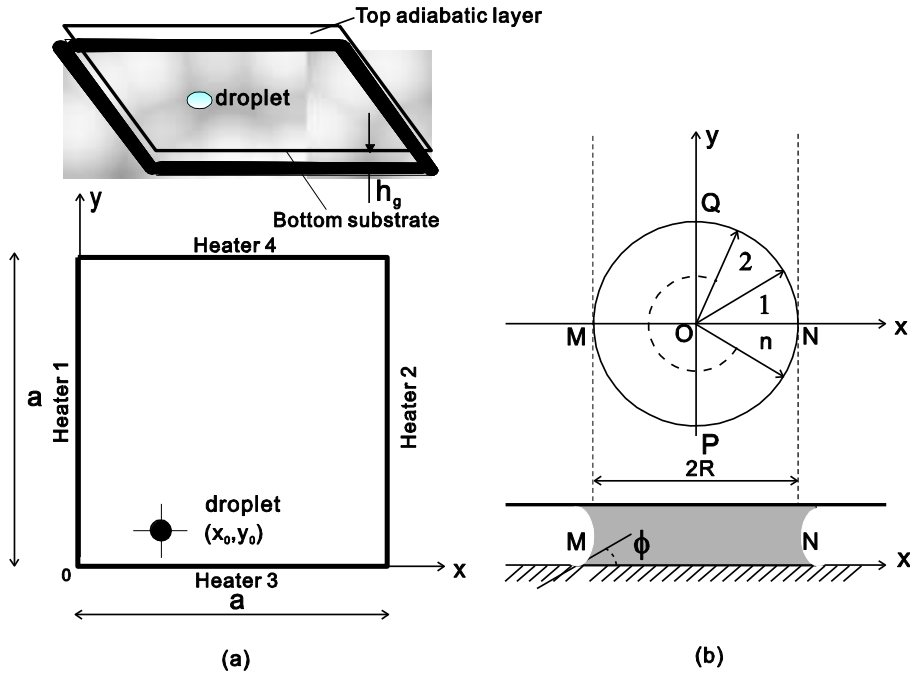

Figure 1. Schematic illustration of thermocapillary actuation of droplet in a planar square platform: (a) The glass plate and heaters; (b) The droplet model.

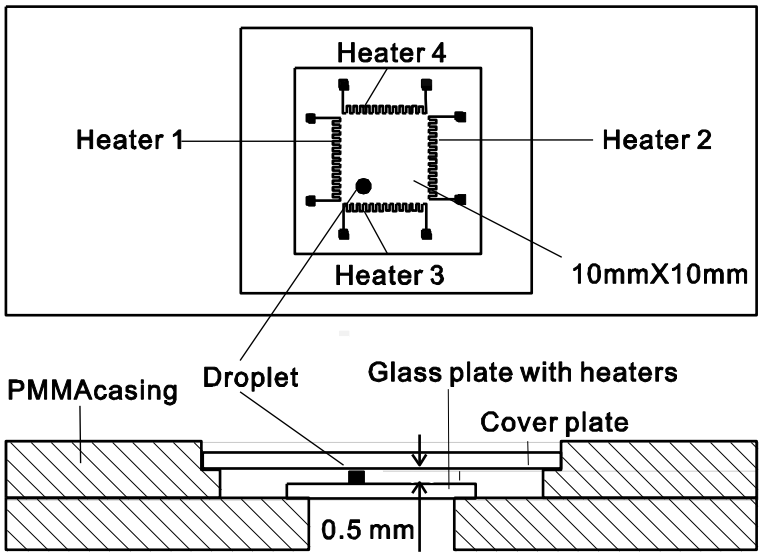

Figure 2. Experimental setup.

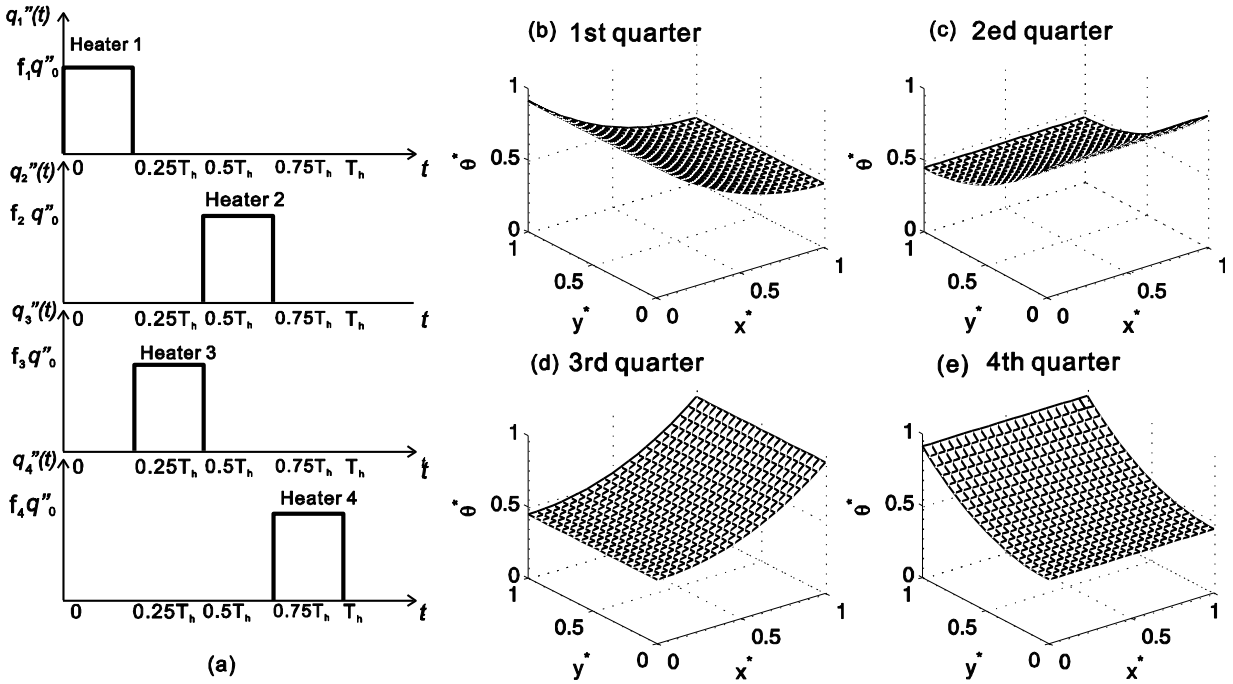

Figure 3. (a) Periodic heating scheme of four heaters in one period. (b)-(e) Temperature distributions corresponding to the heating scheme depicted in (a).

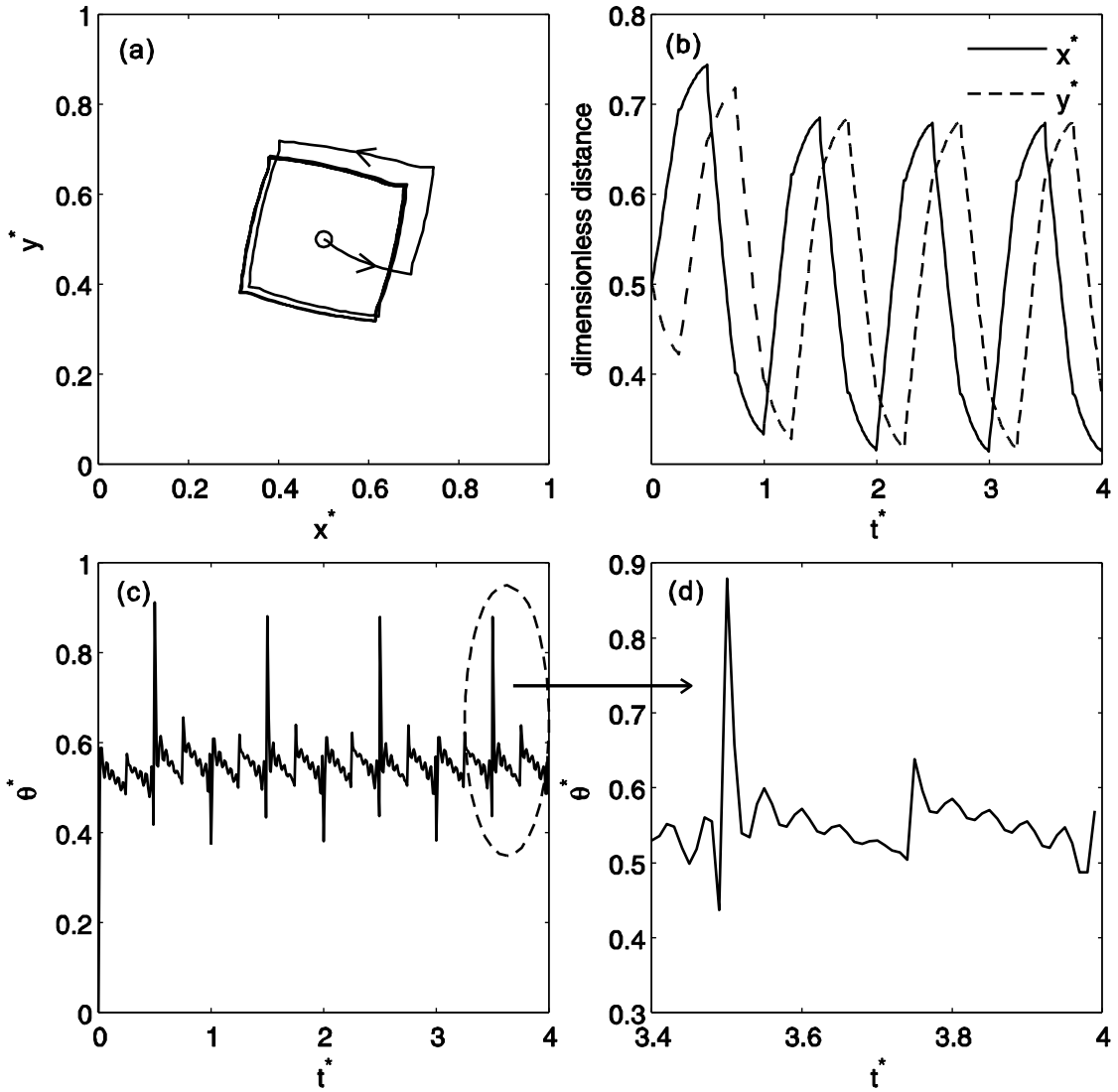

Figure 4. (a) The trajectories of the droplet under the periodic heating scheme described in Figure 3 (a). (b) Dimensionless displacement against dimensionless time in both x and y directions. (c) Dimensionless temperature at the droplet center against dimensionless time. (d) Details of the temperature changes in (c).

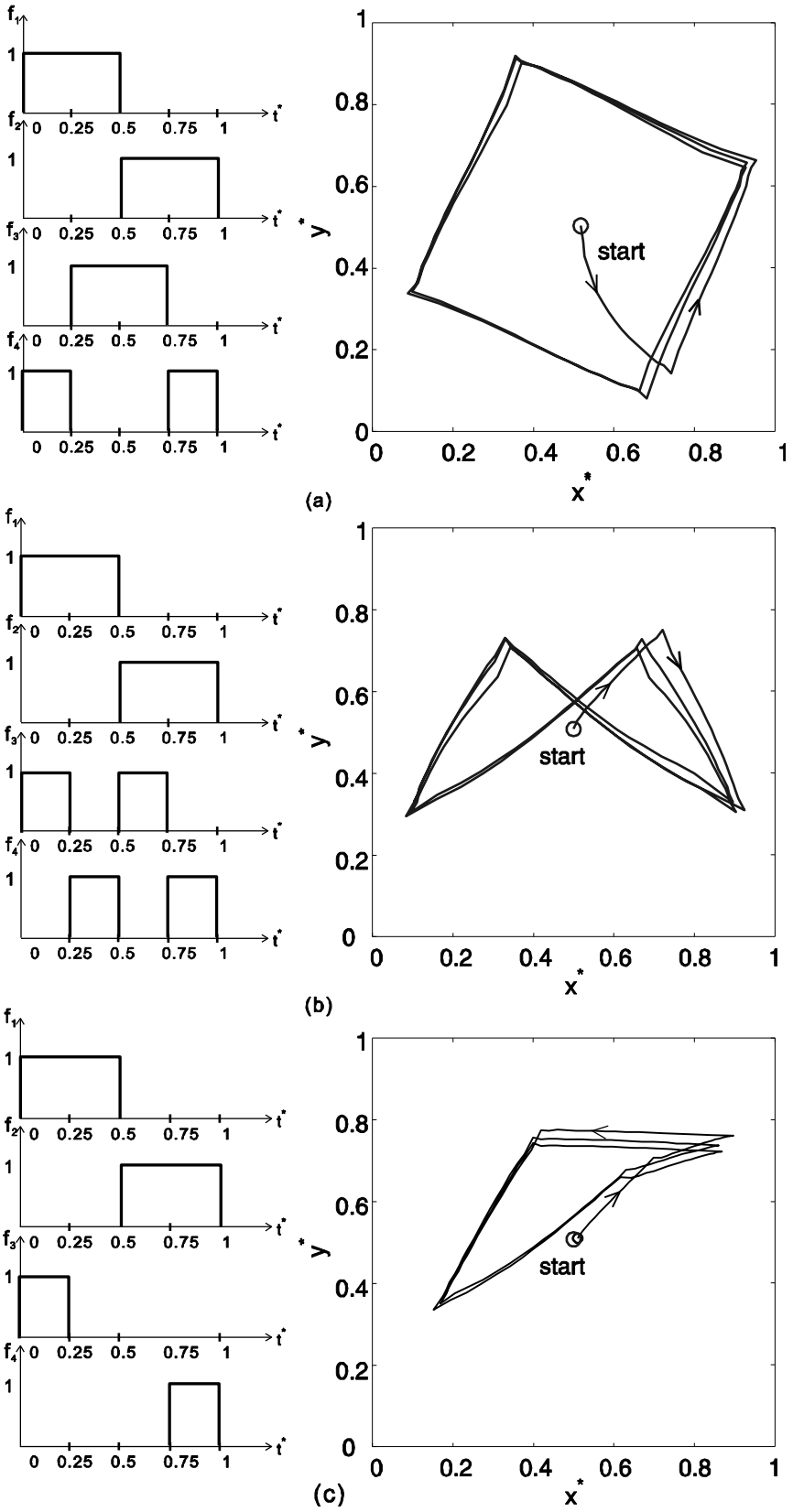

Figure 5. Different periodic heating schemes and the corresponding trajectories.

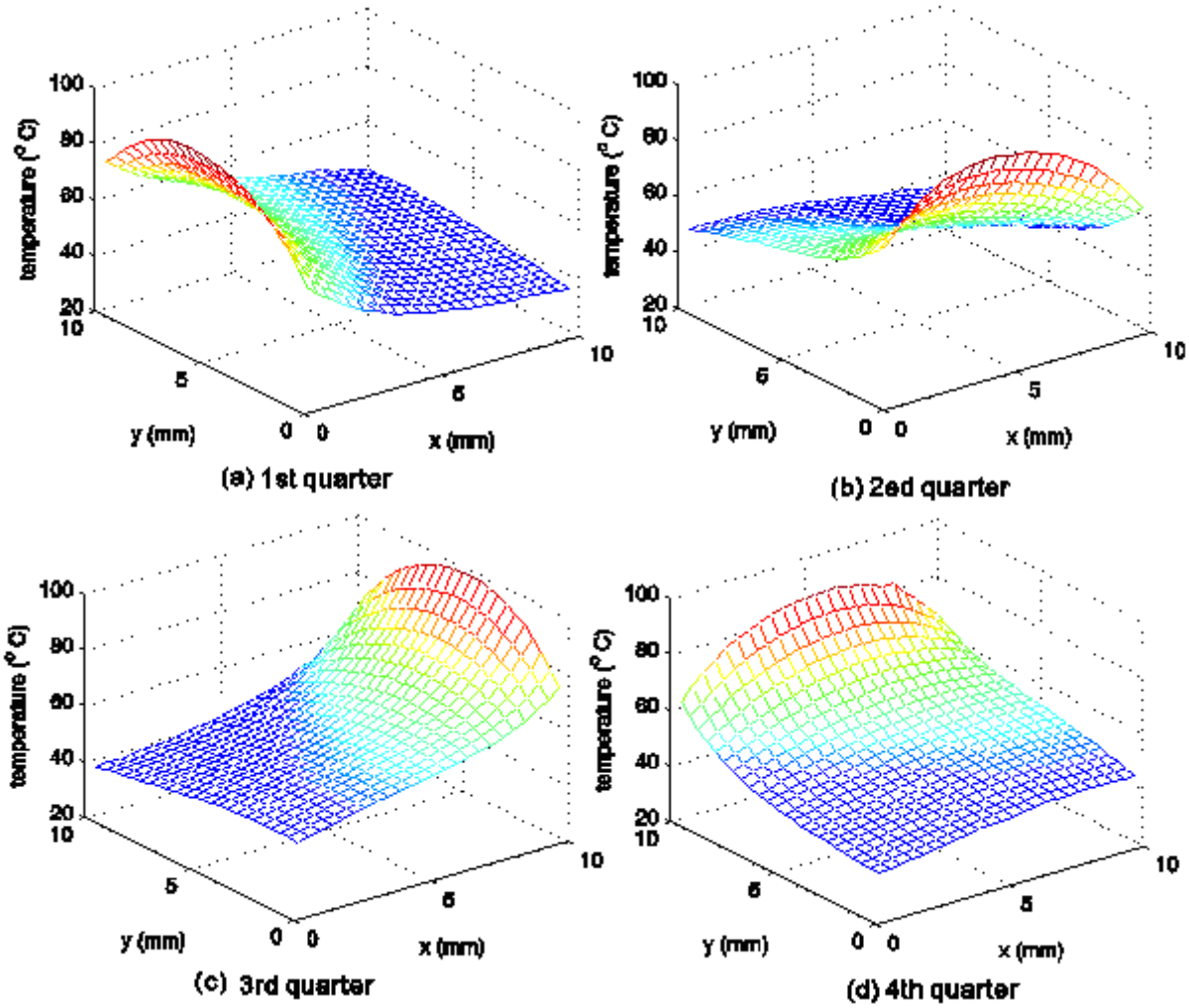

Figure 6. Measured temperature distributions in four quarters of one period corresponding to the heating scheme described in Fig. 3 (a).

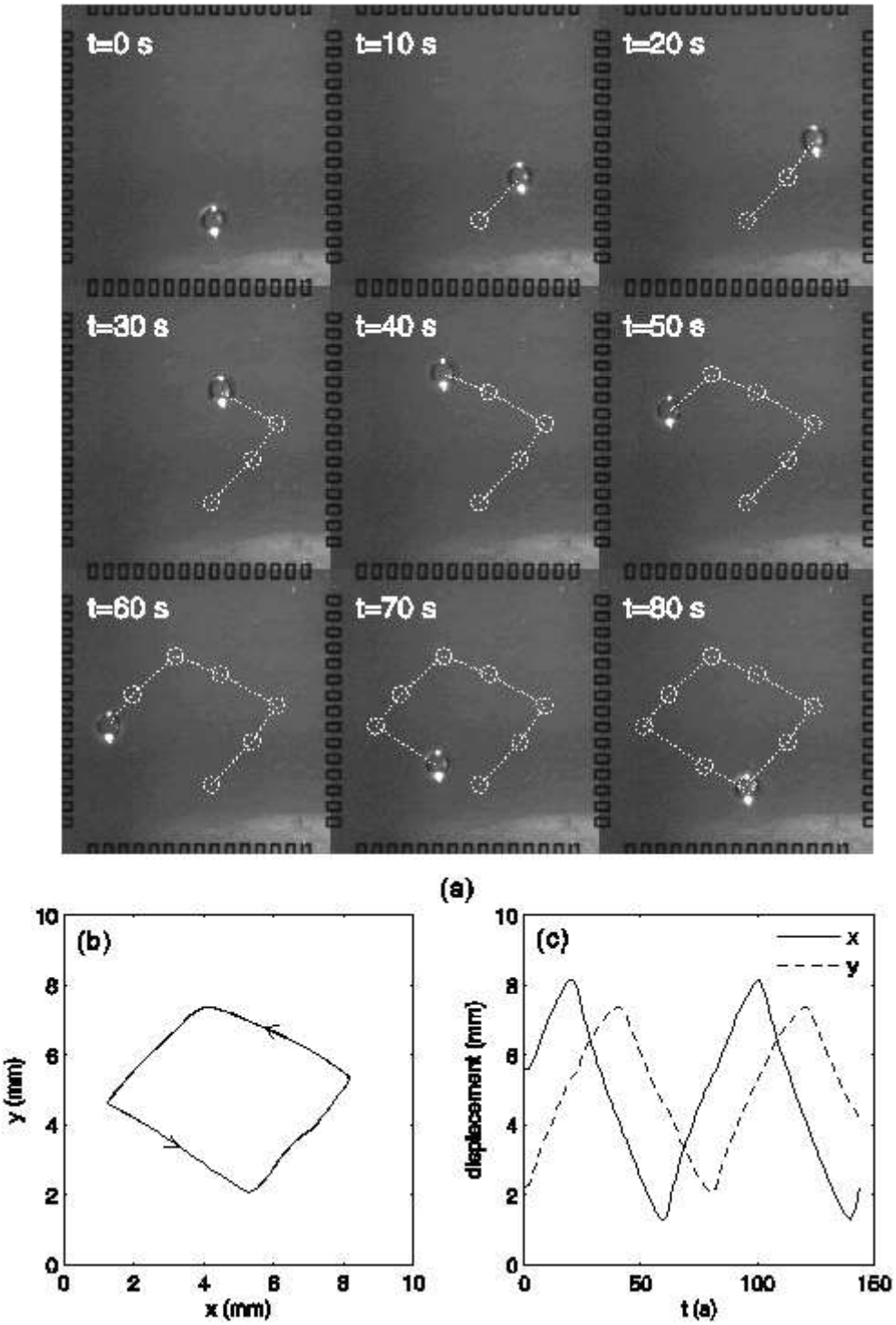

Figure 7. Experimental results under the periodic heating scheme in Figure 3(a) with a period of T_h = 80 s. (a) Selected images of droplet motion; (b) Trajectories; (c) Droplet displacement against time in both *x* and *y* directions.

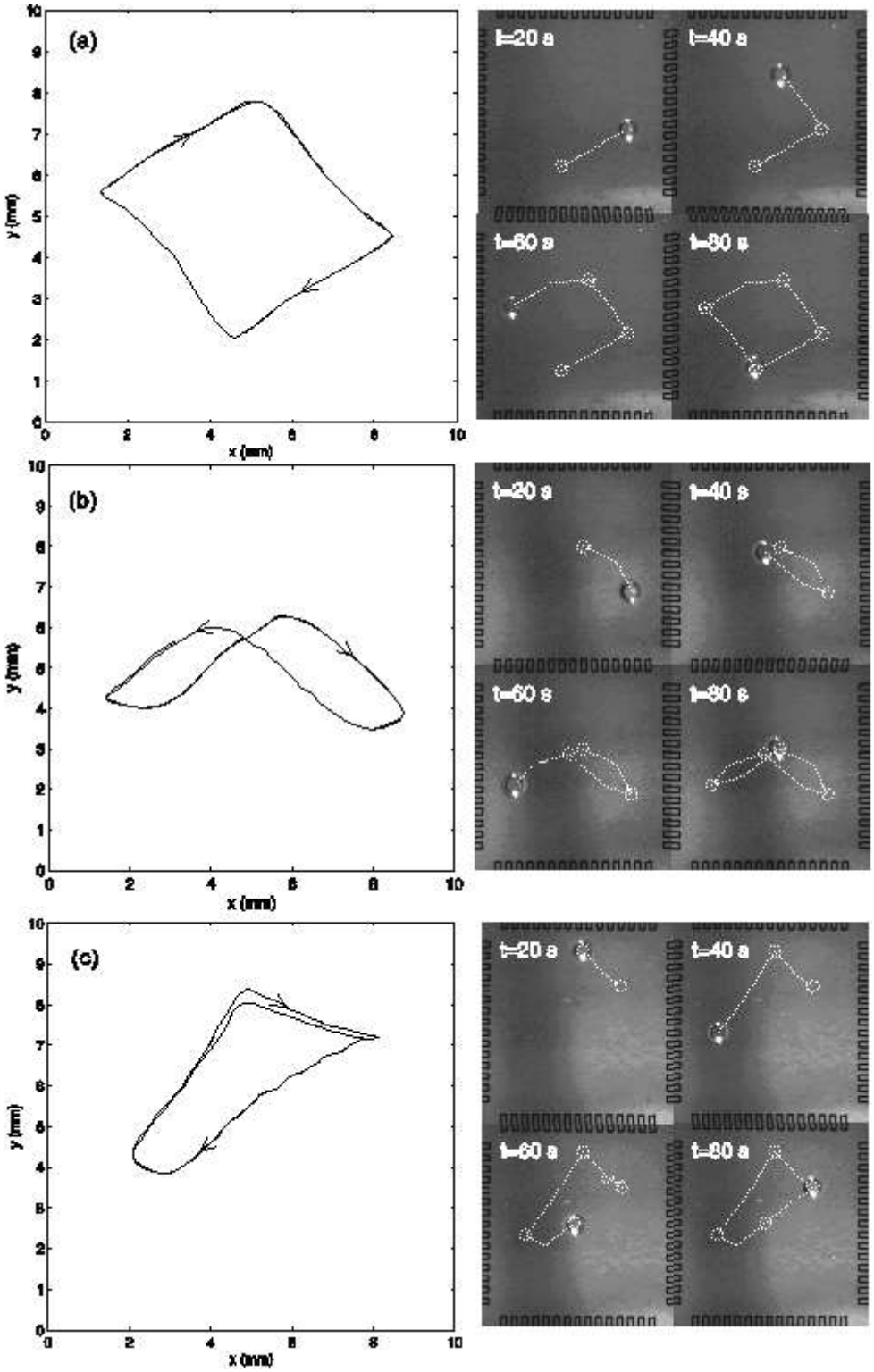

Figure 8. Selected images and trajectories of a droplet under actuation corresponding to the periodic heating schemes described Figures 5(a)-(c), T_h = 80s. The trajectories are obtained from the images recorded for 144s.

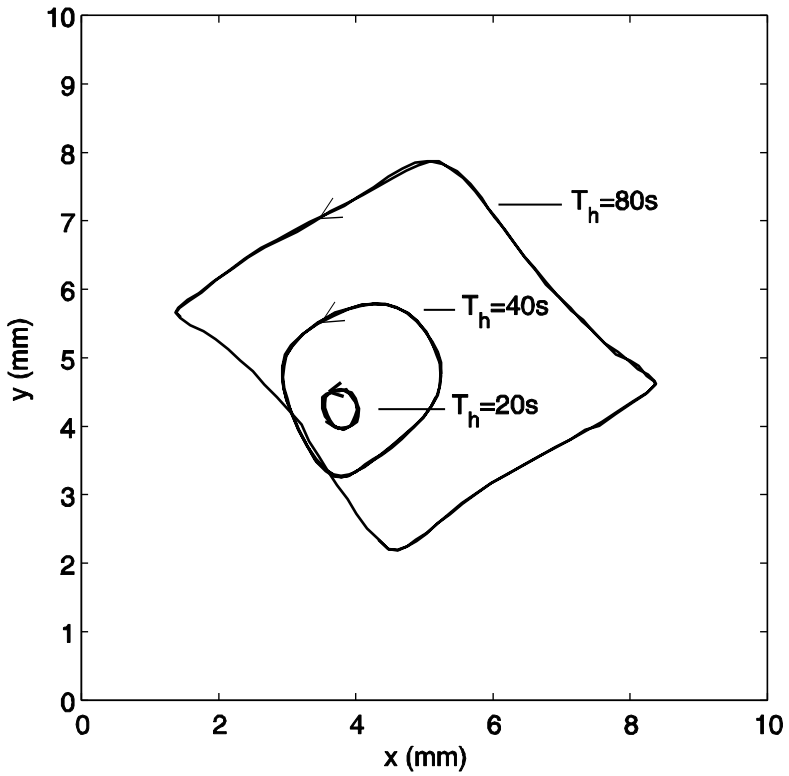

Figure 9. The measured trajectories of a droplet under the heating scheme described Figure 3(a) with different period.